Band flips and bound-state transitions in leaky-mode photonic lattices

Sun-Goo Lee and Robert Magnusson

Phys. Rev. B **99**, 045304 — Published 16 January 2019

DOI: 10.1103/PhysRevB.99.045304

Band flips and bound-state transitions in leaky-mode photonic lattices

Sun-Goo Lee and Robert Magnusson*

(Dated: November 12, 2018)

We present analytical and numerical results on the formation and properties of the leaky stop band in one-dimensional photonic lattices. At the second stop band, one band edge mode suffers radiation loss generating guided-mode resonance whereas the other band edge mode becomes a non-leaky bound-state in the continuum. We show that the frequency location of the leaky band edge, and correspondingly the bound-state edge, is determined by superposition of Bragg processes generated by the first two Fourier harmonics of the spatial dielectric constant modulation. At the closed-band state, we discover an analytic condition for the exceptional point where frequency is fully degenerate.

Periodic subwavelength metastructures, including one-dimensional (1D) and two-dimensional (2D) metagratings in photonic-crystal slab geometry, are governed by principles that depend strongly on the scale of the operational wavelength λ relative to the period Λ. In the deep subwavelength regime $\Lambda \ll \lambda$, classic effective-medium theory [1] becomes accurate and the materials are effectively homogenized enabling facile phase control, anti-reflection properties, and polarization manipulation. In the subwavelength resonance regime with the period moderately smaller than the wavelength $\Lambda < \lambda$, on the other hand, effective-medium theory fails and the metastructures exhibit intricate resonance effects on account of coupling of incident light to quasi-guided lateral Bloch modes [2]. The attendant resonance regime enables a variety of novel device concepts exemplified by wideband reflectors [3], narrow bandpass filters [4], and polarizers [5]. Most of the important properties are associated with the second (leaky) stop band because it admits light injection into the lattice via broadside illumination. Moreover, at the second stop band, only two propagating external (zero order) waves exist and thus energy transfer between them is particularly efficient.

In this Letter, we address fundamental properties of the second band gaps of photonic lattices in the resonance regime. The band structure admits a leaky edge and a non-leaky edge for each supported resonant Bloch mode if the lattice is symmetric. The leaky modes generate various spectral responses via guided-mode resonances (GMRs) and the non-leaky edge becomes a bound-state in the continuum (BIC), or embedded eigenvalue, currently of great scientific interest [6–18]. We show that it is possible to control the width of the leaky band gap by lattice design. In particular, as a modal band closes, there results a degenerate state – this state is remarkable as it is possible to transit to it by parametric and material choice as shown here. We demonstrate that the transition to, and across, the degenerate point executes a band flip. To understand the physical mechanisms inducing the band closure and the band flip, we investigate the band gap formation relative to lattice harmonic content and device parameters by employing a semi-analytical model and finite-difference time-domain (FDTD) simulations [19, 20]. The semi-analytical dispersion model is particularly powerful as it provides direct physical insight into leaky band dynamics including band closure and the degenerate state associated with exceptional points in dispersion.

As noted in Fig. 1(a), we analyse a single 1D periodic layer of thickness d enclosed by a substrate with dielectric constant ϵ_s and a cover region of ϵ_c. The periodic layer acts as a waveguide as well as a phase-matching element because its average dielectric constant $\epsilon_{avg} = \epsilon_l + \rho(\epsilon_h - \epsilon_l) = 4.00$ is larger than $\epsilon_s = 2.25$ and $\epsilon_c = 1.00$, where ϵ_h and ϵ_l represent the high and low dielectric constants, respectively, and where ρ is the fill factor of the high dielectric constant part. We use a parameter $\Delta\epsilon = \epsilon_h - \epsilon_l$ to represent the level of dielectric constant modulation, keeping ϵ_{avg} constant to highlight the effect of changes in $\Delta\epsilon$ clearly. In this 1D case, photonic band gaps open up for media with ϵ_h and ϵ_l when $0 < \rho < 1$ and $\Delta\epsilon > 0$. As shown schematically in Fig. 1(b), leaky modes in blue circles generate GMR effects in the reflection spectra by coupling with the in-

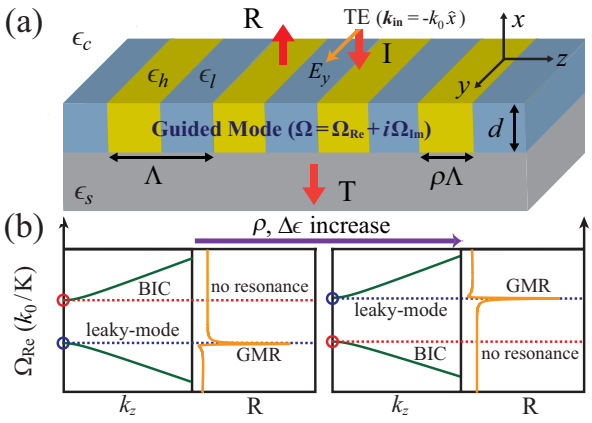

FIG. 1. (color online) (a) Schematic of a 1D photonic lattice with a normally-incident TE-polarized plane wave. (b) Conceptual illustration of the band flip and bound-state transition. Here, k_z is the wavevector along the z-direction and $\mathrm{K} = 2\pi/\Lambda$ is the magnitude of the grating vector. Guided modes are described by complex normalized frequency Ω.

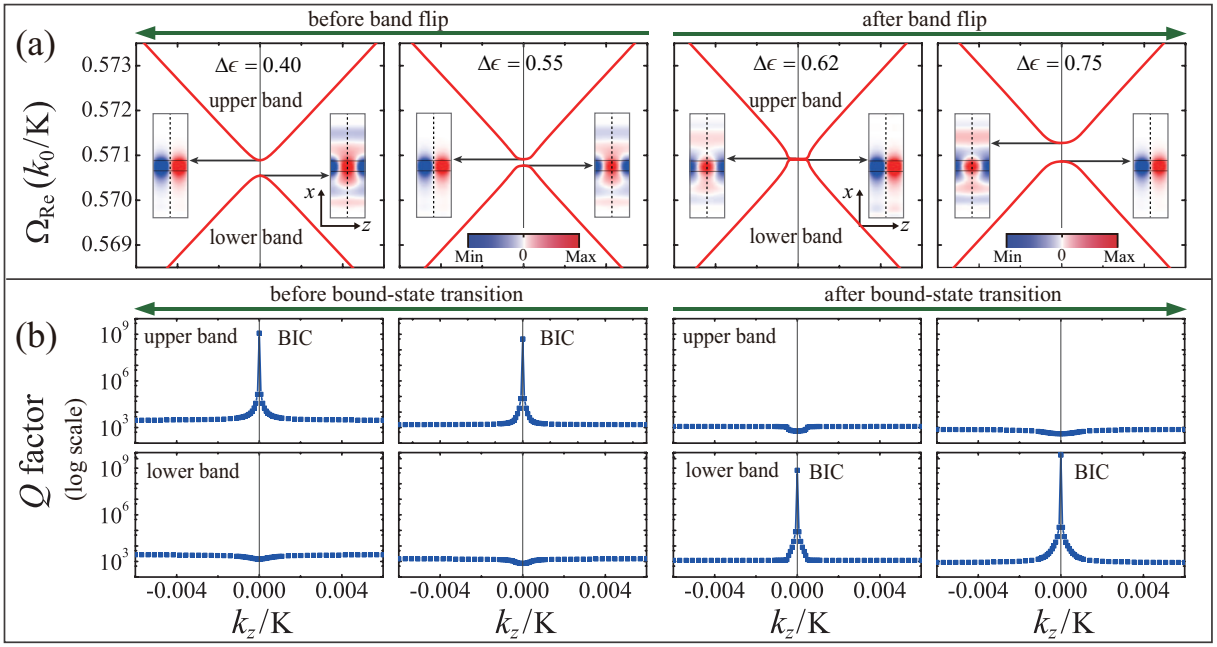

FIG. 2. (color online) Band flip and bound-state transitions in a 1D leaky-mode photonic lattice. (a) FDTD simulated dispersion relations near the second stop band for six different values of $\Delta\epsilon$. Insets with blue and red colors illustrate spatial electric field (E_y) distributions of band edge modes at the $y = 0$ plane. Vertical dotted lines represent the mirror planes in the computational cells. The band gap closes when $\Delta\epsilon = 0.62$. Before and after the band gap closure, spatial field profiles of the band edge modes are reversed. (b) Calculated radiative Q factors of the upper and lower bands. Bound states with asymmetric modal profiles are located in different bands before and after the band gap closure. In the FDTD simulations, we use structural parameters $d = 0.50\ \Lambda, \rho = 0.48, \epsilon_c = 1.00, \epsilon_s = 2.25$, and $\epsilon_{avg} = 4.00$. Details on the FDTD simulations are provided in the Supplemental Materials [22].

cident wave whereas BICs in red circles cannot produce a resonance because they are symmetry protected. The location of the BIC (leaky mode) transfers from the upper (lower) to the lower (upper) band edge due to the band flip effect as ρ and/or $\Delta\epsilon$ increase. In general, if the lattice supports numerous leaky modes, each mode will undergo similar transitions as each mode possesses a band gap [21]. In this study, we limit our attention to the fundamental TE mode as this simplest case brings out the key properties of the band dynamics.

Figure 2(a) shows the evolution of the second stop band under variation of $\Delta\epsilon$ for $\rho = 0.48$. As the value of $\Delta\epsilon$ increases from zero, the band gap opens and its size increases. However, the gap size decreases and becomes zero as $\Delta\epsilon$ is further increased. On additional increase in $\Delta\epsilon$ the band gap reopens and its size grows again. These dynamics are associated with band flip as seen by the spatial profiles of the band edge modes plotted in the insets of Fig. 2(a). When $\Delta\epsilon$ is 0.4 and 0.55, the upper (lower) band edge modes have asymmetric (symmetric) spatial electric field (E_y) distributions. When $\Delta\epsilon$ is 0.62 and 0.75, on the other hand, the upper (lower) modes have symmetric (asymmetric) field distributions. The field computations also show that symmetric band edge modes are radiative out of the grating layer whereas asymmetric modes are well localized in the grating layer. The band transitions associated with the symmetry-protected BIC states are seen clearly in Fig. 2(b) depicting Q factors as a function of k_z. When $\Delta\epsilon$ is 0.4 and 0.55, the BIC state resides in the upper band and the Q factor increases without bound at the center of the first Brillouin zone. Meanwhile, the Q factor in the lower band does not exceed 1500 in the computed region $|k_z/\mathrm{K}| \leq 0.006$. On the contrary, Fig. 2(b) shows that high-Q BIC states exist in the lower band when $\Delta\epsilon$ is 0.62 and 0.75.

We now show that the band flip and inter band transition presented in Fig. 2 is induced by superposition of Bragg processes denoted by $\mathrm{BR}_{q,n}$ where q indicates the Bragg order and n denotes the Fourier harmonic of the dielectric constant modulation. As an approximation, we keep only the strongest Bragg processes which are $\mathrm{BR}_{2,1}$ operating as a second-order Bragg reflection off the first Fourier harmonic and $\mathrm{BR}_{1,2}$ defining a first-order Bragg reflection by the second harmonic. Central to our study is investigating photonic band structures analytically by solving the 1D wave equation given by [23]

$$\left(\frac{\partial^2}{\partial x^2} + \frac{\partial^2}{\partial z^2}\right) E_y(x,z) + \epsilon(x,z) k_0^2 E_y(x,z) = 0, \quad (1)$$

where k_0 denotes the free-space wavenumber. Equation (1) can be solved numerically by expanding the periodic dielectric function $\epsilon(x,z)$ in a Fourier series

and by expanding the electric field E_y as plane waves [24]. For the 1D symmetric lattice, the dielectric function can be expanded in an even cosine function series $\epsilon(z) = \sum_0^\infty \epsilon_n \cos(n\mathrm{K}z)$ where the Fourier coefficients are given by $\epsilon_0 = \epsilon_{avg}$ and $\epsilon_{n\geq 1} = (2\Delta\epsilon/n\pi)\sin(n\pi\rho)$. For clear insight into the leaky-mode band dynamics, we use a simple semi-analytical approach proposed by Kazarinov and Henry (KH); this model is then verified by rigorous FDTD computations. The KH model solves the wave equation by retaining only the zeroth, first, and second Fourier harmonics [25]. The spatial electric field distribution is approximated as $E_y(x,z) = [A\exp(+i\mathrm{K}z) + B\exp(-i\mathrm{K}z)]\varphi(x) + E_{rad}$, where $\varphi(x)$ characterizes the mode profile of the unmodulated waveguide and E_{rad} represents the radiating diffracted wave. Near the second stop band, the dispersion relation can be written as

$$\Omega(k_z) = \Omega_0 - \left(ih_1 \pm \sqrt{k_z^2 + (h_2 + ih_1)^2}\right)/(\mathrm{K}h_0), \quad (2)$$

where Ω_0 is the Bragg frequency under vanishing index modulation and the coupling coefficients are given by

$$h_0 = \Omega \int_{-\infty}^{\infty} \epsilon_0(x)\varphi(x)\varphi^*(x)dx, \quad (3)$$

$$h_1 = i\frac{\mathrm{K}^3\Omega^4\epsilon_1^2}{8}\int_{-d}^{0}\int_{-d}^{0} G(x,x')\varphi(x')\varphi^*(x)dx'dx, \quad (4)$$

$$h_2 = \frac{\mathrm{K}\Omega^2\epsilon_2}{4}\int_{-d}^{0} \varphi(x)\varphi^*(x)dx, \quad (5)$$

where $G(x,x')$ denotes the Green's function for the diffracted field [26, 27], see Supplemental Materials [22] for details.

To check the validity of the stop band formation by the Bragg processes, we calculate the band structures of pertinent 1D lattices by FDTD simulations. In Fig. 3(a), the stop band denoted $\Delta\Omega_1$ is formed by $\mathrm{BR}_{2,1}$ with $\epsilon(z) = \epsilon_0 + \epsilon_1\cos(\mathrm{K}z)$. Dispersion curves (blue lines) obtained from the full non-approximated lattice are also plotted for comparison. Clearly, the FDTD results with the fundamental harmonic only are quite different from those with the full lattice. Figure 3(b) shows stop band $\Delta\Omega_2$ formed by $\mathrm{BR}_{1,2}$. The full-lattice band structure is close to the approximate structure denoting the importance of this partial scattering process. Figure 3(c) shows that the third order harmonic cannot contribute to the second stop band by itself. Figure 3(d) illustrates that the band $\Delta\Omega_{12}$ simulated with the first and second harmonics simultaneously agrees well with the band $\Delta\Omega$ simulated with the full non-approximated lattice. Moreover, there is excellent agreement with the dispersion curves calculated with the KH model. Hence, we conclude that the Bragg-reflection superposition model proposed here is valid to describe the second stop band of weakly to moderately modulated photonic lattices.

Equation (2) indicates that the leaky stop band with two band edges $\Omega^a = \Omega_0 + h_2/(\mathrm{K}h_0)$ and $\Omega^s = \Omega_0 - (h_2 + i2h_1)/(\mathrm{K}h_0)$ opens at $k_z = 0$. At the band edge with frequency Ω^a, which is obtained when the electric field distribution is an asymmetric (sine) function ($A = -B$), there is no radiation loss because Ω^a is purely real. At the Ω^s band edge obtained when the field distribution is a symmetric (cosine) function ($A = B$), the radiative loss is maximal with $\mathrm{Im}(\Omega^s) = -2\mathrm{Re}(h_1)/(\mathrm{K}h_0)$. Hence, the band edge modes with the frequencies Ω^a and Ω^s are associated with the BIC and GMR, respectively.

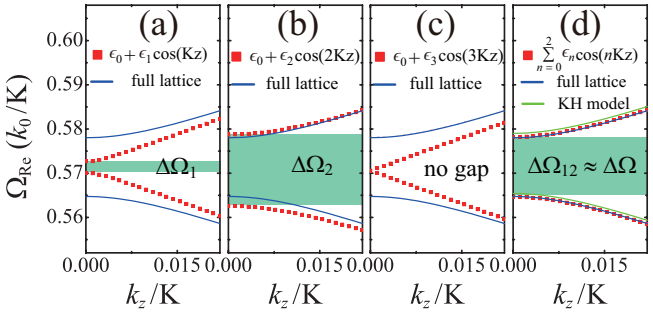

FIG. 3. (color online) Computed stop bands for a 1D leaky-mode lattice relative to Fourier harmonic content. The dielectric functions vary for these examples. (a) $\epsilon = \epsilon_0 + \epsilon_1\cos(\mathrm{K}z)$, (b) $\epsilon = \epsilon_0 + \epsilon_2\cos(2\mathrm{K}z)$, and (c) $\epsilon = \epsilon_0 + \epsilon_3\cos(3\mathrm{K}z)$. In (d) $\epsilon = \epsilon_0 + \epsilon_1\cos(\mathrm{K}z) + \epsilon_2\cos(2\mathrm{K}z)$ is used. Parameters for the FDTD simulations and KH model are $d = 0.50\ \Lambda, \rho = 0.35, \epsilon_c = 1.00, \epsilon_s = 2.25, \Delta\epsilon = 1.00$, and $\epsilon_{avg} = 4.00$.

Since the coupling coefficients h_1 and h_2 are due to the first and second Fourier harmonics, respectively, superposition between the scattering processes $\mathrm{BR}_{2,1}$ and $\mathrm{BR}_{1,2}$ can be understood from the two coupling coefficients. For the symmetric lattice shown in Fig. 1(a), h_2 is positive (negative) when the fill factor ρ is smaller (greater) than 0.5; this happens because the second Fourier harmonic coefficient $\epsilon_2 = (\Delta\epsilon/\pi)\sin(2\pi\rho)$ changes its sign once from + to − when $\rho = 0.5$. But $\mathrm{Im}(h_1)$ is always positive irrespective of ρ. Since the size of the band gap is given by $\mathrm{Re}(|\Omega^a - \Omega^s|) = 2|h_2 - \mathrm{Im}(h_1)|$, when $\rho > 0.5$ with $h_2 < 0$, the size of the gap results from the constructive interference of $\mathrm{BR}_{2,1}$ and $\mathrm{BR}_{1,2}$. When $\rho < 0.5$, on the other hand, the gap size is determined by the destructive interference of $\mathrm{BR}_{2,1}$ and $\mathrm{BR}_{1,2}$ and thus the gap size can reach a zero value. Fill-factor-dependent interplay between $\mathrm{BR}_{2,1}$ and $\mathrm{BR}_{1,2}$ can be also understood from FDTD simulated spatial electric field distributions of band edge modes at $\Delta\Omega_1$ and $\Delta\Omega_2$, see Fig. S3 in Supplemental Materials [22].

When both ρ and $\Delta\epsilon$ are small, the non-leaky asymmetric BIC locates at the upper band edge because the first order reflection $\mathrm{BR}_{1,2}$ dominates the second order reflection $\mathrm{BR}_{2,1}$. But when ρ increases and approaches 0.5, there is a chance for $\mathrm{BR}_{2,1}$ to overwhelm $\mathrm{BR}_{1,2}$ because the strength of $\mathrm{BR}_{1,2}$ gets weaker and becomes zero as ϵ_2 approaches zero. For a given value of ρ (< 0.5), as $\Delta\epsilon$ increases from zero there should exist a critical value

of index modulation $\Delta\epsilon_{\mathrm{BF}}$ where the band gap closes and the bound-state transition takes place. Before (After) the band gap closure, BICs should appear at upper (lower) band edges. As the value of ρ gets closer to 0.5, a smaller value of index modulation $\Delta\epsilon$ will be required for $\mathrm{BR}_{2,1}$ and $\mathrm{BR}_{1,2}$ to balance each other because the coupling coefficients h_1 and h_2 are proportional to $\epsilon_1^2 = [2\Delta\epsilon/\pi \times \sin(\pi\rho)]^2$ and $\epsilon_2 = \Delta\epsilon/\pi \times \sin(2\pi\rho)$, respectively. Table I shows simulated $\Delta\epsilon_{\mathrm{BF}}$ for five different fill factors. It is seen that $\Delta\epsilon_{\mathrm{BF}}$ increases from 0.31 to 1.55 when ρ decreases from 0.49 to 0.45. The dependence of $\Delta\epsilon_{\mathrm{BF}}$ on ρ shown in Table I coincides with the prediction of the destructive interaction between $\mathrm{BR}_{1,2}$ and $\mathrm{BR}_{2,1}$.

Band transitions of symmetry-protected BICs at $k_z = 0$ can be found in 1D leaky-mode photonic lattices which have 180° rotational symmetry around the x-axis (C_2^x) and time reversal symmetry (T). In the transition process with the variation of $\Delta\epsilon$ shown in Fig. 2, the topological charge carried by the symmetry-protected BIC is maintained because $C_2^x T$ symmetry is preserved and there is no creation or annihilation of BIC since our lattice has no up-down mirror symmetry [7, 28].

When a leaky band closes as shown in Fig. 2(a) with $\Delta\epsilon = 0.62$, there exists a finite range of Bloch wave vectors Δk_z where $\partial\Omega_{\mathrm{Re}}/\partial k_z = 0$. Leaky band flattening with band gap closure is related to the exceptional point where the real part Ω_{Re} and imaginary part Ω_{Im} of frequency are fully degenerated simultaneously [29, 30]. When the band gap closes with $h_2 = \mathrm{Im}(h_1)$, the dispersion relation in Eq. (2) can be rewritten as

$$\Omega(k_z) = \Omega_0 - \left(ih_1 \pm \sqrt{k_z^2 - \mathrm{Re}(h_1)^2}\right)/(\mathrm{K}h_0). \qquad (6)$$

Equation (6) clearly shows that frequency is fully degenerate at $k_{ex} = \pm\mathrm{Re}(h_1)$. Near the exceptional point, comparing with linear dependency, the square-root dependence of the leaky dispersion relations is expected to induce a large change in frequency with a small variation of k_z. Hence, exceptional points in 1D leaky bands have been proposed to increase the sensitivity of GMR devices [30].

Out-of-plane radiation at the leaky edge with a bound state at the opposing edge are primary aspects of the leaky-mode photonic lattices under study herein. Band flips and bound-state transitions have been formulated above. We also investigated non-leaky stop bands in conventional periodic stack lattices with infinite thickness. Figure S1 in the Supplemental Materials [22] shows that the dispersion curves cross as straight lines and $\partial\Omega_{\mathrm{Re}}/\partial k_z \neq 0$ at $k_z = 0$ when the non-leaky stop band closes. However, we verified band flip at the non-leaky band edges in terms of electric-field distributions.

TABLE I. $\Delta\epsilon_{\mathrm{BF}}$ as a function of ρ. As ρ decreases from 0.5, the modulation strength $\Delta\epsilon_{\mathrm{BF}}$ increases. In the FDTD simulations, $\Delta\epsilon$ was increased in discrete steps of 0.01 and $\Delta\epsilon_{\mathrm{BF}}$ is defined as the first value where the band flip is observed.

ρ	0.49	0.48	0.47	0.46	0.45
$\Delta\epsilon_{\mathrm{BF}}$	0.31	0.62	0.93	1.24	1.55

In summary, we investigated band flips and bound-state transitions in 1D photonic lattices. Our analysis show that the second band gap is primarily controlled by first-order Bragg diffraction by the second Fourier harmonic lattice component. However, near fill-factor of 0.5, second-order Bragg diffraction by the fundamental Fourier harmonic becomes competitive with the primary process. It is the destructive interference of these major two processes that closes the gap and induces a band flip whereby the leaky edge and the bound-state edge transit across the band gap. Thus, these fundamental Bragg processes control the band dynamics. Consequently, the band does not close at fill factor being identically 0.5 as often assumed. As the grating modulation strength increases, the transition point is increasingly pulled away from this value. An exceptional point is identified at the closed gap on account of the powerful semi-analytical dispersion model applied. Our study is limited to the simplest possible 1D lattice without up-down mirror symmetry. Therefore, topological charge carried by the bound state is conserved during the transition process. Whereas our work elucidates fundamental aspects of the band dynamics of leaky-mode photonic lattices, the basic methodology presented can be applied in other device architectures including photonic-crystal slabs and metamaterials.

This material is based upon work supported by the National Science Foundation under Grant no. ECCS-1606898. Additional support was provided by the Texas Instruments Distinguished University Chair in Nanoelectronics endowment.

* Department of Electrical Engineering, University of Texas at Arlington, Box 19016, Arlington, Texas 76019, USA; magnusson@uta.edu

[1] S. M. Rytov, Sov. Phys. JETP **2**, 466–475 (1956).
[2] Y. H. Ko and R. Magnusson, Optica **5**, 289-294 (2018).
[3] P. Moitra, B. A. Slovick, W. Li, I. Kravchencko, D. P. Briggs, S. Krishnamurthy, and J. Valentine, ACS Photonics **2**, 692–698 (2015).
[4] M. Niraula, J. W. Yoon, and R. Magnusson, Opt. Lett. **40**, 5062–5065 (2015).
[5] Y. Ding and R. Magnusson, Opt. Express **12**, 5661–5674 (2004).
[6] J. Gomis-Bresco, D. Artigas and L. Torner, Nature Photonics **11**, 232–236 (2017).
[7] C. W. Hsu, B. Zhen, A. D. Stone, J. D. Joannopoulos, and M. Soljačić, Nature Reviews Materials **1**, 1–13 (2016).
[8] D. C. Marinica, A. G. Borisov, and S. V. Shabanov, Phys.

Rev. Lett. **100**, 183902 (2008).
[9] C. W. Hsu, B. Zhen, J. Lee, S.-L. Chua, S. G. Johnson, J.D. Joannopoulos, and M. Soljačić, Nature **449**, 188–191 (2013).
[10] M. G. Silveirinha, Phys. Rev. A **89**, 023813 (2014).
[11] Y. Yang, C. Peng, Y. Liang, Z. Li, and S. Noda, Phys. Rev. Lett. **113**, 037401 (2014).
[12] F. Monticone and A. Alù, Phys. Rev. Lett. **122**, 213903 (2014).
[13] Y. Plotnik, O. Peleg, F. Dreisow, M. Heinrich, S. Nolte, A. Szameit, and M. Segev, Phys. Rev. Lett. **107**, 183901 (2011).
[14] E. N. Bulgakov and A. F. Sadreev, Physc. Rev. A **90**, 053801 (2014).
[15] J. Lee, B. Zhen, S. Chua, W. Qiu, J. D. Joannopoulos, M. Soljačić, and O. Shapira, Phys. Rev. Lett. **109**, 0067401 (2012).
[16] X. Gao, C. W. Hsu, B. Zhen, M. Soljačić, and H. Chen, arXiv:1707.01247 (2017).
[17] A. Kodigala, T. Lepetit, Q. Gu, B. Bahari, Y. Fainman, and B. Kanté, Nature **541**, 196–199 (2017).
[18] H. M. Doeleman, F. Monticone, W. den Hollander, A. Alú, and A. F. Koenderink, Nat. Photonics **12**, 397–401 (2018).
[19] A. Taflove, *Computational Electrodynamics: The Finite-Difference Time-Domain Method* (Artech House, Boston, 1995).
[20] A. F. Oskooi, D. Roundy, M. Ibanescu, P. Bermel, J. D. Joannopoulos, and S. G. Johnson, Comput. Phys. Commun. **181**, 687–702 (2010).
[21] R. Magnusson and M. Shokooh-Saremi, Optics Express, **16**, 3456–3462 (2008).
[22] See Supplemental Material for (1) Finite-difference time-domain simulations; (2) Band flips in a non-leaky 1D photonic lattice; (3) Semi-analytical calculation of dispersion relation; (4) Field distributions of band edge modes.
[23] A. Yariv and P. Yeh, *Optical Waves in Crystals* (Wiley, New York, 1984).
[24] K. Inoue and K. Ohtaka, *Photonic Crystals: Physics, Fabrication and Applications* (Springer-Verlag Berlin Heidelberg, 2004.).
[25] R. F. Kazarinov and C. H. Henry, IEEE J. Quant. Electronics **21**, 144–150 (1985).
[26] Y. Ding and R. Magnusson, Opt. Express **15**, 680–694 (2007).
[27] D. Rosenblatt, A. Sharon, and A. A. Friesem, IEEE J. Quant. Electronics **33**, 2038–2059 (1997).
[28] B. Zhen, C. W. Hsu, L. Lu, A. D. Stone, and M. Soljačić, Phys. Rev. Lett. **113**, 257401 (2014).
[29] B. Zhen, C. W. Hsu, Y. Igarashi, L. Lu, I. Kaminer, A. Pick, S.-L. Chua, J. D. Joannopoulos, and M. Soljačić, Nature (London) **525**, 354–358 (2015).
[30] W. Chen, S. K. Ozdemir, G. Zhao, J. Wiersig, and L. Yang, Nature **548**, 192–196 (2017).